JOURNAL OF EXPERIMENTAL AND THEORETICAL PHYSICS, 2024, Vol. 166, No. 5(11), pp. 678–684

ORDER, DISORDER, AND PHASE TRANSITION IN CONDENSED MEDIA

SPECTRA OF RESONANT MAGNETOPLASTICITY IN NaCl(Ca + Ni) CRYSTALS

© 2024 V. I. Alshits*, M. V. Koldaeva, E. A. Petrzhik, E. V. Darinskaya

Shubnikov Institute of Crystallography of the Kurchatov Complex of Crystallography and Photonics of the National Research Center "Kurchatov Institute", Moscow, 119333 Russia

**e-mail: valshits@mail.ru*

Received July 12, 2024

Revised July 16, 2024

Accepted July 19, 2024

Abstract. The resonant spectrum of dislocation paths in a NaCl(Ca+Ni) crystal has been measured under ultra-low crossed magnetic fields, the constant Earth field and alternating pump field. The movement is caused by spindependent transformation of impurity stoppers on dislocations, leading to their depinning and relaxation displacements in the field of internal stresses. The spectrum of resonant pump field frequencies is interpreted in terms of hyperfine interaction of electron pairs at impurity centers and surrounding Cl ligands. The spectrum is compared with previously obtained spectra: of microhardness on the same crystal and of dislocation paths in NaCl(Ca) crystal. Similarities and differences among the three spectra provide establishing the relative role of Ca and Ni impurities in the observed processes.

DOI: 10.31857/S004445102411e129

1. INTRODUCTION

It has now been reliably established [1–5] that the effect of magnetic fields on non-magnetic crystals leads to changes in their mechanical properties. This phenomenon, called the magnetoplastic effect (MPE), consists in the spin-dependent transformation of point defects in magnetic fields. It is physically analogous to the well-known spin-dependent influence of magnetic field on the rate of chemical reactions [6, 7]. Naturally, magnetic modification of impurities in crystals should affect not only their mechanical properties but also other properties sensitive to doping. Thus, magnetic sensitivity has been discovered in dark conductivity [8], and optical properties of semiconductors [9], and defect formation processes in near-surface silicon layers under thermal shock conditions [10], as well as dielectric properties of ferroelectrics and ferroelastics [11–16].

Both *in situ* effects, when changes occur directly during magnetic exposure, and memory effects, when the response occurs after the fields are turned off, are observed. In relation to MPE, magnetostimulated changes in dislocation mobility are usually studied as *in situ* effects. In memory effects, the response to magnetic influences is most often used in the form of changes in crystal microhardness. The nature of these phenomena is identical. In both cases, the initial transformation of defects is associated with spin-dependent electronic transitions in them directly in the magnetic field [5, 17–20]. The new state of defects, which are stoppers for dislocations, leads to immediate depinning of dislocations and their further movement in internal stress fields. In memory effects, the change in defect structure in the magnetic field occurs throughout the crystal volume, but this usually does not immediately lead to changes in macro-properties. First, equilibrium is disturbed, for example, local electroneutrality, which causes diffusive relaxation of lattice around defects and determines relatively slow changes in crystal microhardness.

One of the effective methods of magnetic influence is the exposure of crystals to crossed magnetic fields – constant and perpendicular to it alternating pump field. In this case, the change in mechanical properties has a resonant character. The first experimental results were obtained in [21–25] at frequencies typical for EPR ~10 GHz. Peaks

of dislocation paths or microhardness (NaCl) and starting stresses for dislocations (Si) were measured. Their corresponding magnetic field values B (at fixed pump frequency ν_{res}) were described by the usual condition

$$\nu_{res} = g\frac{\beta B}{h}, \quad (1)$$

where β – Bohr magneton, h – Planck constant, B – permanent magnetic field component (~0.3 T) and $g \approx 2$ – Lande factor. In NaCl(Eu) crystals [22, 23] under classical EPR conditions, microhardness peaks were observed at field values B, ocorresponding to known regions of EPR activity.

Later, similar resonances were discovered and studied at much lower frequencies, around 1 MHz using Earth's magnetic field of about 50 μT as a constant component of crossed fields [26–33]. Resonance magnetically stimulated changes in microhardness in this range were discovered in various crystals [28, 30–32]. A characteristic feature of these low-frequency resonances, distinguishing them from the usual range, is anisotropy: the resonant frequency of the effect proved to be sensitive to the crystal orientation relative to the magnetic field **B**. In particular, when rotating a NaCl sample by θ an angle relative to the magnetic field around the 4-th order symmetry axis, the resonant frequency of dislocation mobility is determined by the modified formula [28]

$$\nu_{res} = g\frac{\beta B}{h}\cos\theta. \quad (2)$$

As shown in [31], dependence (2) is maintained for microhardness of very complex crystals of triglycine sulfate (TGS), potassium hydrogen phthalate (KAP) and zinc oxide (ZnO). In this work it was shown for the first time that the value θ has a simple physical meaning: it is the angle between the external field **B** and the local internal field $\mathbf{B}_{loc}$ under conditions where $B \ll B_{loc}$,

$$\theta = \angle(B, B_{loc}). \quad (3)$$

And the directions of local fields $\mathbf{B}_{loc}$ are associated with crystal symmetry elements [32, 33].

In NaCl crystal, the calcium (Ca), impurity usually predominates entering the crystal as a non-magnetically active ion Ca^{2+} adjacent to sodium vacancy V_{Na} (for local electroneutrality). In this crystal, memory effects usually do not manifest themselves. And only on the dislocation the transformation into a paramagnetic state, $Ca^{2+} \rightarrow Ca^{+}$, occurs [5, 29, 33]. It is believed that such rapid diffusionless self-organization of the stopper structure in the dislocation core occurs as follows. When a dislocation approaches the "dumbbell" $Ca^{2+}V_{Na}$, the ion Na^{+} is displaced from the edge of the extra-plane of the dislocation core by enormous pressure to the vacancy site, and from the nearest to Ca^{2+} ion Cl^{-} in the same core, Coulomb forces transfer an electron to calcium: $Ca^{2+} \rightarrow Ca^{+}$.

However, memory effects can be observed in NaCl when adding magnetically active impurity. For example, in NaCl(Ca+Ni) crystal a whole spectrum (18 peaks) of microhardness changes was obtained [32] after exposing samples in the EPR scheme in Earth's magnetic field.

It should be noted that in an earlier study [29] on the same NaCl(Ca+Ni) crystal, where the Ni concentration was significantly lower than Ca, the dislocation mobility in a constant magnetic field was significantly higher than in a crystal without Ni. The solution to this paradox was based on the hypothesis that Ni impurity in NaCl crystal in the absence of a magnetic field is a significantly stronger stopper than Ca. In this work, for the first time, we will present the measured resonance spectrum of dislocation paths in NaCl(Ca+Ni) crystal in the same range as the microhardness spectrum [32]. Comparing these spectra with each other and with a fragment of a similar dislocation spectrum in NaCl(Ca) crystal without Ni [33], we will, among other things, show that the hypothesis mentioned in [29] was correct.

2. METHODOLOGY

The studies were conducted on NaCl(Ca+Ni) crystals with specially introduced nickel impurity, grown at LOMO by the Kyropoulos method. According to the trace impurity analysis performed using the PerkinElmer Total Quant method, the crystals contain 2 ppm Ni. The total content of all other impurities was about 10 ppm, among which calcium predominates. For comparison, NaCl(Ca) crystals of the same origin with similar composition but without nickel addition were used. Samples were cleaved along cleavage planes {100} in the form of parallelepipeds with approximate dimensions $3 \times 3 \times (5-8)$ mm, after which they were annealed and chemically polished. The annealing was carried

out in argon atmosphere at 750°C for five days and ended with very slow cooling [1, 5]. This reduced the initial dislocation density and significantly increased the average path length of freshly introduced dislocations during their magnetic relaxation.

As an external impact, crossed magnetic fields were used: the Earth's field B_{Earth} and a perpendicular pump field $\tilde{B}$. The magnitude and direction of the Earth's magnetic field were measured directly at the sample location in the setup. The field vector $\mathbf{B}_{Earth}$ formed an angle 29.5°, with the vertical, and its magnitude was equal to $B_{Earth} = 49.9$ μT. A concentric variable magnetic field was created in a coaxial chamber around a wire through which a sinusoidal alternating current of a given frequency was passed. In this work, the frequency varied in the range of 1.1–2.2 MHz. The amplitude $\tilde{B}$ was approximately 3 μT. Note that, according to [27], changing the orientation of the pump field $\bar{\mathbf{B}}$ in this EPR variant does not affect the position of the resonance frequency (2), however, it reduces the relaxation mobility of dislocations. But even with parallel fields $\bar{\mathbf{B}}$ and $\mathbf{B}_{Earth}$ the resonance effect remains quite measurable.

When studying dislocation mobility, fresh dislocations were introduced into the samples by a light impact just before the experiment, which with this method of introduction are mainly straight with orientation along the directions $\mathbf{L} \parallel [100]$. Magnetic exposure was carried out for 5 minutes. The sample was positioned so that the studied dislocations were perpendicular to both the constant field ($\mathbf{B}_{Earth} \parallel [001]$), and the variable field ($\mathbf{B} \parallel [010]$) (see, for example, [27] for details). The initial and final positions of dislocations were fixed by selective chemical etching. Observations were made for edge dislocations. Their average run l was determined from a sufficiently large number of displacements 50–300. We will characterize it by the dimensionless parameter $l\sqrt{\rho}$, equal to the ratio of the run l to the average distance $1/\sqrt{\rho} \sim 100$ μm between dislocations, where ρ is their average density ($\rho \sim 10^4$ cm^{-2}).

The methodology for measuring microhardness H of the same crystal, the results of which are used below for comparisons, is described in [32]. We only note that the methodology used in these experiments made it possible to reduce the error in determining relative changes in microhardness $\Delta H/H_0$ to 1%. This was achieved by increasing the statistical base of measurements through plotting curves of hardness dependence on time after exposure. The minimum on such a smooth curve was a well-reproducible experimental point.

3. EXPERIMENTAL RESULTS AND THEIR DISCUSSION

A comparison was made between two responses of NaCl(Ca+Ni) crystal to the effect of crossed magnetic fields in an EPR-type setup in Earth's constant field while varying the pumping field frequency ν. In both cases, magnetically stimulated crystal softening was observed. One response was the displacement of dislocations $l\sqrt{\rho}$ in magnetic fields without any additional mechanical impacts, and the other was a decrease in crystal hardness $\Delta H/H_0$ after its magnetic exposure. Both dislocation mobility and hardness changes have a resonant character. Figure 1 shows three compared dependencies in the same frequency range: the spectrum of microhardness changes $\Delta H/H_0(\nu)$ of the NaCl(Ca+Ni) crystal [32] (Fig. 1*a*), the spectrum of dislocation paths $l\sqrt{\rho}(\nu)$ in the same crystal obtained in this work (Fig. 1*b*) and a similar path dependence $l\sqrt{\rho}$ for NaCl(Ca) crystal [33] (Fig. 1*c*).

It should be noted that each spectrum contains two groups of peaks consisting of 9 resonances. They are marked in Fig. 1: A_n and $\widehat{A}_n$, B_n and $\widehat{B}_n$, C_n and $\widehat{C}_n$. In work [32], it was noted that the resonant frequencies in these groups (ν_n^A for peaks A_n and $\hat{\nu}_n^A$ for $\widehat{A}_n$), marked in Fig. 1*a* are interconnected by relation $\hat{\nu}_n^A \approx \nu_n^A/\sqrt{2}$. Near each peak in Fig. 1, there are corresponding symbols. In terms of formulas (2) and (3), provided that the direction of the external field $\mathbf{B}_{Earth} \parallel [001]$ remains constant, these groups correspond to two directions of the local magnetic field $\mathbf{B}_{loc} \parallel < 100 >$ and $\mathbf{B}_{loc} \parallel < 110 >$ along the symmetry axes of 4th and 2nd order, forming an angle $\hat{\theta}_n^A = 45°$ with each other (certainly, with accuracy up to small local distortions near defects). It turned out that the same relation holds for two other spectra. The table shows the corresponding angles $\hat{\theta}_n^A$, $\hat{\theta}_n^B$ and $\hat{\theta}_n^C$ (3) between the external field $\mathbf{B}_{Earth}$ and local field $\mathbf{B}_{loc}$ close to the corresponding axis 2, calculated using formula

$$\hat{\theta}_n^{A,B,C} = \arccos(\hat{\nu}_n^{A,B,C}/\nu_n^{A,B,C}). \qquad (4)$$

Their small deviations from 45° are caused not only by measurement errors but also by natural

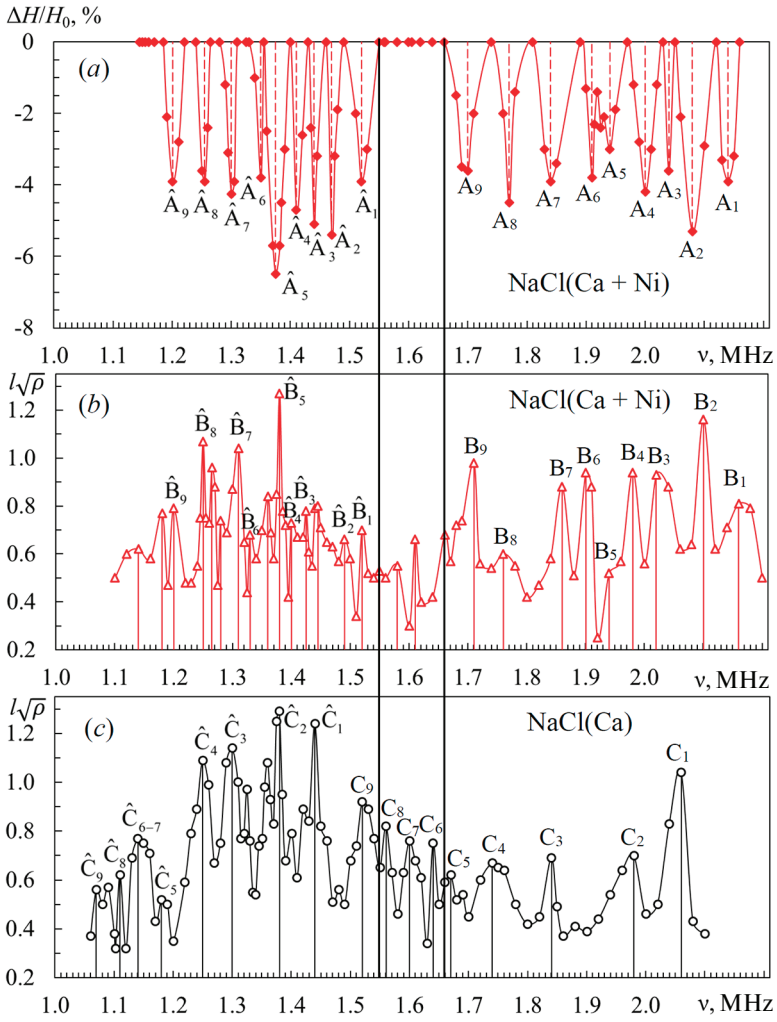

Fig. 1. Frequency dependencies of relative changes in microhardness (*a*) and normalized average dislocation path (*b*, *c*) of NaCl(Ca + Ni) (*a*, *b*) and NaCl(Ca) (*c*) crystals. Samples were kept in crossed magnetic fields for 30 minutes (a), 5 minutes (*b*, *c*)

lattice distortions near the paramagnetic defect. Nine corresponding effective g-factors g_n^A, g_n^B and g_n^C in the table, calculated using formula (2) at $\theta = 0$, apparently are determined by hyperfine interaction of impurity centers with ligands (Cl nuclei around them). According to the table, they are close for the spectra in Figs. 1*a* and *b*, belonging to one crystal. A small difference between them (within 1%) may be related to differences in the structure of the impurity environment in the bulk and in the dislocation core. And the values in the third spectrum differ quite significantly (about 10%) from the first two, since this time we are dealing with different paramagnetic centers in the environment of the same ligands.

There is no doubt that the first spectrum (Fig. 1*a*) is caused by the presence of only Ni impurity in the crystal, sin Ca^{2+} ions are diamagnetic. The Ni^{2+} ion, like the Ca^{2+}, ion, has no electrons in the outer shell, but it has two unpaired electrons in the *d*-shell, so it is paramagnetic even outside dislocations.

The third spectrum (Fig. 1*c*) just as undoubtedly reflects processes associated with Ca impurity. Ca impurity in the form of a non-magnetically active ion Ca^{2+} at the dislocation transforms with the participation of a vacancy into a paramagnetic state $Ca^{2+} \rightarrow Ca^{+}$ [5], and therefore participates in spin-dependent processes under a magnetic field, including in the EPR scheme.

Table 1. Resonance frequencies $\nu_n^{A,B,C}$ and $\hat{\nu}_n^{A,B,C}$ (in MHz), as well as effective g-factors $g_n^{A,B,C}$ and angles (4) $\hat{\theta}_n^{A,B,C}$ for three spectra in Fig. 1

Crystal	Test	Group	1	2	3	4	5	6	7	8	9
NaCl (Ca + Ni)	Hardness	g_n^A	3.058	2.972	2.915	2.858	2.772	2.729	2.629	2.529	2.429
		ν_n^A	2.14	2.08	2.04	2.00	1.94	1.91	1.84	1.77	1.70
		$\hat{\nu}_n^A$	1.52	1.49	1.425	1.40	1.38	1.33	1.31	1.25	1.20
		$\hat{\theta}_n^A$	44.7°	44.2°	45.7°	45.6°	44.7°	45.9°	44.6°	45.1°	45.1°
	Dislocations	g_n^B	3.087	3.001	2.887	2.830	2.772	2.715	2.658	2.515	2.444
		ν_n^B	2.16	2.10	2.02	1.98	1.94	1.90	1.86	1.76	1.71
		$\hat{\nu}_n^B$	1.52	1.49	1.425	1.40	1.38	1.33	1.31	1.25	1.20
		$\hat{\theta}_n^B$	45.3°	44.8°	45.1°	45.0°	44.7°	45.6°	45.2°	44.7°	45.4°
NaCl (Ca)	Dislocations	g_n^C	2.944	2.829	2.630	2.486	2.387	2.344	2.287	2.229	2.172
		ν_n^C	2.06	1.98	1.84	1.74	1.67	1.64	1.60	1.56	1.52
		$\hat{\nu}_n^C$	1.44	1.38	1.30	1.25	1.18	1.14		1.11	1.07
		$\hat{\theta}_n^C$	45.7°	45.8°	45.0°	44.1°	45.0°	46.0°	44.6°	44.6°	45.3°

The second spectrum reflects the relaxation motion of dislocations through a set of Ca and Ni pinning centers, while the concentration of the former is 5 times higher than the latter. This is the very paradox that we discussed in [29]. As can be seen from the spectrum in Fig. 1*b*, it contains not only peaks of groups B_n and $\widehat{B}_n$, similar to the spectrum in Fig. 1*a*, but also others, weaker ones, similar to the spectrum in Fig. 1*c*.

In reality, one should remember that we are working with well-annealed crystals, in which Ca atoms should be gathered in complexes, while Ni atoms are few and they most likely remain single. Therefore, the number of pinning centers of two types may be comparable or even in favor of Ni. Furthermore, if the pinning force of Ni impurity is notably stronger than that of Ca, then when introducing fresh dislocations, they will stop in places with higher internal stresses, where Ca complexes do not "hold" dislocations. Apparently, this is why the dislocation spectrum of the NaCl(Ca+Ni) crystal (Fig. 1*b*), mainly almost coincides with Fig. 1*a*, as if there were no Ca complexes at all.

Nevertheless, Ca complexes quite distinctly manifest themselves in the spectrum in Fig. 1*b*. This is most clearly seen in the frequency range (1.56–1.66 MHz, marked by vertical lines in Fig. 1), where there is no resonance effect in the case of microhardness. For dislocations, resonant depinning with "switched off" Ni is carried out by Ca atoms. This can occur in crystal regions with lower internal stresses, where dislocation pinning is carried out by both Ni and Ca impurities, so that magnetically stimulated depinning of dislocations from Ca can lead to its displacement. It is these rather weak peaks that are visible in this part of the spectrum, approximately in the same place as the peaks in Fig. 1*c*. It should be noted that a completely analogous situation arises at $\nu < 1.19$ MHz to the left of the last peak $\widehat{A}_9$ in Fig. 1*a*. Here again, Ca impurities manifest themselves in Fig. 1*b* by resonant peaks that are close in position to the peaks in Fig. 1*c*.

Questions about the more detailed features of phenomena underlying the observed effects can only be answered hypothetically for now. For example, why does the change in the structure of such small defects as Ni impurity, especially when present in such low concentrations, cause such strong macroscopic consequences as changes in crystal hardness. Perhaps because in NaCl crystals, indentation is accompanied by plastic deformation in the form of dislocation loops and their movement in specific "rosettes". In this case, the decrease in hardness would be directly related to the increase in dislocation mobility, as shown in the spectrum in Fig. 1*b*. However, in the latter case, the transformation of the stopper on the dislocation occurs almost instantaneously, while the maximum changes in microhardness are observed with a significant delay (~2 h). Possibly, the transformation of the pinning center in the dislocation core occurs without delay, due to extreme pressures that ensure

rapid diffusionless self-organization of the structure (see example in Introduction), while in the bulk, slow diffusion processes are required for the necessary structural self-organization.

Of course, there is still a significant lack of specifics regarding the details of the elementary act of spin-dependent transformation of impurity centers even in such model crystals as NaCl. So far, we describe them only in the most general terms. When the crystal is held in crossed magnetic fields, spin-dependent electronic transitions occur in the radical pair formed by an electron at the impurity center and an electron on the chlorine ion [5, 17–20, 28, 33]. These become possible due to the lifting of the Pauli exclusion principle. The radical pair can transit from S state to T (and then the pinning center decays) or vice versa, from T to S (and then a new product is formed). Which specific process occurs remains unclear, but according to our experimental data, in this case, magnetic exposure leads to pinning decrease.

4. CONCLUSIONS

Analysis of frequency spectra obtained on NaCl(Ca+Ni) crystals using different experimental techniques, and their comparison with the spectrum of dislocation paths in NaCl(Ca) confirmed that two types of magnetoplastic effect (*in situ* and memory) have a common nature. As can be seen from Figure and the table, the resonant frequencies in the NaCl(Ca+Ni) crystal for in situ effect and memory effect are very close. Spin-dependent electronic transitions occur directly in the magnetic field. The transformation of impurity complexes, on which dislocations are pinned, occurs rapidly and leads to the depinning of dislocations and their further movement in internal stress fields. These dislocation displacements are measured in in situ experiments. In experiments with microhardness measurements in NaCl(Ca+Ni) crystal after the described resonant transition with a change in the Ni-center structure, subsequent diffusion relaxation to a new local equilibrium occurs, which in turn modifies such a macro characteristic of the crystal as hardness. Thus, using various experimental techniques (studying dislocation mobility and measuring microhardness), it is possible to separate the contributions of each impurity in the case of crystals with a two-component impurity system.

In conclusion, it should be noted that during the long period of academic research of MPE, a significant amount of new fundamental knowledge has been accumulated [1–5, 17–35] at an increasingly deeper level of understanding of subtle physical processes. Studies of this phenomenon are highly non-trivial due to the fact that the elementary act of transforming the structure of the impurity center and the observed macroscopic consequences of this have too different scales. As a result, it is necessary to build a strategy of various indirect measurements that complement each other and establish causal relationships along this path. The present work demonstrates a small example of such a strategy. Nevertheless, it can be stated that a parallel process of gradual implementation of this knowledge into practical technological processes of magnetic treatment of materials in modern technology is being formed before our eyes (see, for example, review [36]).

FUNDING

The work was carried out within the framework of the state assignment of the National Research Center “Kurchatov Institute”.

REFERENCES

1. *V.I. Alshits, E.V. Darinskaya, M.V. Koldaeva, E.A. Petrzhik*, Crystallography **48**, 826 (2003).
2. *A.A. Urusovskaya, V.I. Alshits, A.E. Smirnov, N.N. Bekkauer*, Crystallography **48**, 855 (2003).
3. *Yu.I. Golovin*, FTT **46**, 769 (2004).
4. *R.B. Morgunov*, UFN **174**, 131 (2004).
5. *V.I. Alshits, E.V. Darinskaya, M.V. Koldaeva, and E.A. Petrzhik*, Magnetoplastic effect in nonmagnetic crystals. In: Dislocations in Solids, v. 14, Ch. 86, Ed. J.P. Hirth, Elsevier, Amsterdam (2008), p. 333-437.
6. *A.L. Buchachenko, R.Z. Sagdeev, K.Z. Salikhov*, Magnetic and Spin Effects in Chemical Reactions, Nauka, Novosibirsk (1978).
7. *Ya.B. Zeldovich, A.L. Buchachenko, E.L. Frankevich*, UFN **155**, 3 (1988).
8. *I.S. Volchkov, V.M. Kanevsky, M.D. Pavlyuk*, JETP Letters **107**, 276 (2018).
9. *R. Redko, G. Milenin, V. Milenin, R. Konakova, S. Redko, P. Lytvyn and O. Babenko*, Materials Research Express **6**, 036413 (2019).
10. *A.A. Skvortsov, D.E. Pshonkin, M.N. Luk'yanov*, Key Engineering Materials **771**, 124 (2018).
11. *E.A. Petrzhik, E.S. Ivanova, V.I. Alshits*, Bulletin of the Russian Academy of Sciences: Physics **78**, 1305 (2014).

12. *E.S. Ivanova, E.A. Petrzhik, A.P. Eremeev, R.V. Gainutdinov, A.K. Lashkova, A.G. Ivanova, T.R. Volk*, Crystallography **68**, 738 (2023).

13. *E.D. Yakushkin*, JETP Letters **99**, 483 (2014).

14. *E.D. Yakushkin*, JETP Letters **117**, 598 (2023).

15. *M.N. Levin, V.V. Postnikov, M. Yu. Palagin*, FTT **45**, 1680 (2003).

16. *O.M. Golitsyna, S.N. Drozhdin*, Ferroelectrics **567:1**, 244 (2020).

17. *A.L. Buchachenko*, JETP **129**, 909 (2006).

18. *A.L. Buchachenko*, JETP **132**, 673 (2007).

19. *R.B. Morgunov, A.L. Buchachenko*, JETP **136**, 505 (2009).

20. *R.B. Morgunov and A.L. Buchachenko*, Phys. Rev. B **82**, 014115 (2010).

21. *Yu.I. Golovin, R.B. Morgunov, V.E. Ivanov, S.E. Zhulikov, A.A. Dmitrievsky*, JETP Letters **68**, 400 (1998).

22. *Yu.I. Golovin, R.B. Morgunov, V.E. Ivanov, A.A. Dmitrievsky*, JETP **117**, 1080 (2000).

23. *Yu.I. Golovin, R.B. Morgunov, and A.A. Baskakov*, Molecular Physics **100**, 1291 (2002).

24. *Yu.A. Osipyan, R.B. Morgunov, A.A. Baskakov, A.M. Orlov, A.A. Skvortsov, E.N. Inkina, J. Tanimoto*, JETP Letters **79**, 158 (2004).

25. *M.V. Badylevich, V.V. Kveder, V.I. Orlov, and Yu.A. Osipyan*, Phys. Status Solidi C **2**, 1869 (2005).

26. *V.I. Alshits, E.V. Darinskaya, V.A. Morozov, V.M. Kats, A.A. Lukin*, JETP Letters **91**, 97 (2010).

27. *V.I. Alshits, E.V. Darinskaya, M.V. Koldaeva, E.A. Petrzhik*, FTT **55**, 318 (2013).

28. *V.I. Alshits, E.V. Darinskaya, M.V. Koldaeva, E.A. Petrzhik*, JETP Letters **104**, 362 (2016).

29. *V.I. Alshits, E.V. Darinskaya, M.V. Koldaeva, E.A. Petrzhik*, JETP **149**, 136 (2016).

30. *V.I. Alshits, E.V. Darinskaya, M.V. Koldaeva, E.A. Petrzhik*, FTT **54**, 305 (2012).

31. *V.I. Alshits, M.V. Koldaeva, E.A. Petrzhik*, JETP Letters **107**, 650 (2018).

32. *E.A. Petrzhik, V.I. Alshits*, JETP Letters **113**, 678 (2021).

33. *M.V. Koldaeva and V.I. Alshits*, AIP Advances **14**, 015015 (2024).

34. *X. Zhanga and Z.P. Cai*, JETP Letters **108**, 23 (2018),

35. *Y. Guo, Y.J. Lee, Y. Zhang, A. Sorkin, S. Manzhos, and H. Wang*, Journal of Material Science and Technology **112**, 96 (2022).

36. *Y. Song, W. Wu, Y. Yu, and L. Hua*, Chinese Journal of Mechanical Engineering **36**, 139 (2023).